Synthesis and characterization of a biodegradable elastomer featuring a dual crosslinking mechanism

Richard T. Tran,[a] Paul Thevenot,[a] Dipendra Gyawali,[a] Jung-Chih Chiao,[b] Liping Tang[a] and Jian Yang*[a]

Received 25th January 2010, Accepted 8th March 2010
First published as an Advance Article on the web 21st April 2010
DOI: 10.1039/c001605e

The need for advanced materials in emerging technologies such as tissue engineering has prompted increased research to produce novel biodegradable polymers elastic in nature and mechanically compliant with the host tissue. We have developed a soft biodegradable elastomeric platform biomaterial created from citric acid, maleic anhydride, and 1,8-octanediol, poly(octamethylene maleate (anhydride) citrate) (POMaC), which is able to closely mimic the mechanical properties of a wide range of soft biological tissues. POMaC features a dual crosslinking mechanism, which allows for the option of the crosslinking POMaC using UV irradiation and/or polycondensation to fit the needs of the intended application. The material properties, degradation profiles, and functionalities of POMaC thermoset networks can all be tuned through the monomer ratios and the dual crosslinking mechanism. POMaC polymers displayed an initial modulus between 0.03 and 1.54 MPa, and elongation at break between 48% and 534% strain. *In vitro* and *in vivo* evaluation using cell culture and subcutaneous implantation, respectively, confirmed cell and tissue biocompatibility. POMaC biodegradable polymers can also be combined with MEMS technology to fabricate soft and elastic 3D microchanneled scaffolds for tissue engineering applications. The introduction of POMaC will expand the choices of available biodegradable polymeric elastomers. The dual crosslinking mechanism for biodegradable elastomer design should contribute to biomaterials science.

1 Introduction

A major roadblock in the successful application of synthetic materials in tissue engineering is the lack of suitable scaffolding biomaterials that are able to closely match the mechanical properties of the natural tissue.[1] The mechanical irritation resulting from the compliance mismatch between the scaffold and native tissue leads to inflammation and scar formation, which ultimately prevents the implant from being effectively integrated with the surrounding tissue.[2–6] Many of the biological tissues are soft and elastic in nature with elastic moduli ranging from 20 kPa for cardiac tissue up to 90 kPa for nervous tissue.[7,8] The successful engineering of these tissues demands the development of compliant materials that are mechanically similar to the native tissue, and are able to withstand deformations without causing irritation to their surrounding.[5,9–11] Unfortunately, the FDA approved devices derived from polylactones, such as poly(L-lactide) (PLA), poly(glycolide) (PGA), and their copolymers (PLGA), are stiff and incompliant, which limit their use in soft tissue engineering applications.[12–14] As a result, many groups have focused on the synthesis, characterization, and application of materials with a wide range of biodegradable and elastomeric properties for the development of compliant scaffolds.[1,15–17]

Of the available materials, many of the current hydrogels show potential as materials for drug delivery and tissue engineering scaffolds due to their tissue like mechanical compliance, mass transfer properties, and excellent biocompatibility.[18,19] Hydrogels with elastic properties and that are capable of retaining large amounts of water have been shown to resemble the physical characteristics of the extracellular matrix (ECM) for many soft tissues, thus enhancing their biocompatibility.[19,20] However, major limitations to some of the current hydrogels are the lack of mechanical strength, inability to degrade in a reasonable amount of time due to large number of carbon-carbon crosslinks, and the inability to fine tune their material properties.[21] For example, many of poly(ethylene glycol) (PEG) based hydrogels have been widely used in many biomedical applications, but have poor mechanical strength and show very slow degradation rates.[21,22] To overcome these limitations, polymers such as poly(glycerol-*co*-sebacate) acrylate (PGSA), poly(propylene fumarate) (PPF), and PEG sebacate diacrylate (PEGSDA) are all hydrogels which have improved their mechanical properties and degradation profile by introducing hydrophilic degradable copolymers into the polymer network.[21,23,24]

In this paper, we describe the synthesis and characterization of a novel biodegradable polymer based upon citric acid, maleic anhydride, and 1,8-octanediol, referred to as poly(octamethylene maleate (anhydride) citrate) (POMaC), which features a dual crosslinking mechanism (DCM): carbon-carbon crosslinking *via* ultraviolet (UV) photopolymerization and/or ester bond crosslinking *via* post-polycondensation. Similar to other hydrogels, the UV crosslinking offers advantages such as short reaction times, and allows for the ability to fabricate a wide range of possible scaffold geometries.[25,26] Unlike many other hydrogels, POMaC polymers are able to preserve valuable pendant

[a]*Department of Bioengineering, The University of Texas, Arlington, TX, 76019, USA. E-mail: jianyang@uta.edu; Fax: +817-272-2251; Tel: +817-272-0561*
[b]*Department of Electrical Engineering, The University of Texas, Arlington, TX, 76019, USA*

functional groups, which are reactive moieties amenable to modification with a wide variety of biologically relevant factors to provide opportunities to control cell adhesion and function.[27] The available pendant functional groups can also be utilized to strengthen the polymer network through the formation of degradable ester bond crosslinks.[6] POMaC polymers are versatile in that the photopolymerization can be completely avoided if desired, and crosslinking through polycondensation can be applied to form a thermoset elastomer. Thus, POMaCs provide multiple options to process the polymer network, and allows one to balance the photocrosslinking and polycondensation through the DCM to tailor the material properties of the resulting elastomer to fit a wide range of soft tissue engineering applications.

POMaCs have the following advantages: the use of non-toxic monomers, a simple synthesis that can be conducted under mild conditions, controllable mechanical and degradable properties, and easy processability. The rationale behind the biomaterial design are: (1) using the concept that collagen and elastin are crosslinked polymers that provide elasticity to the natural ECM, we chose crosslinking as a mechanism to confer elasticity to the biomaterial; (2) to increase the manufacturing potential, we chose to use inexpensive monomers and a cost-effective synthesis procedure performed under mild heating without the use of any catalysts. Citric acid, maleic anhydride, and 1,8-octanediol are inexpensive and have been used in many other biomaterials for tissue engineering.[6,28–34] Citric acid is a versatile monomer that participates in pre-polymer formation through a simple polycondensation reaction while preserving pendant functionality; (3) the incorporation of ester bonds into the polymer backbone confers degradability to the crosslinked polymer network; (4) to allow for a wide control over the mechanical properties, degradation, and functionality of the biomaterial, we chose to incorporate a DCM; and (5) the feed ratio of the monomers, polymer concentration, and post-polymerization time can also be used to fine-tune the material properties of the polymer. Thus as a platform biomaterial, POMaCs are novel biodegradable elastomers with tunable properties for potential use in soft tissue engineering.

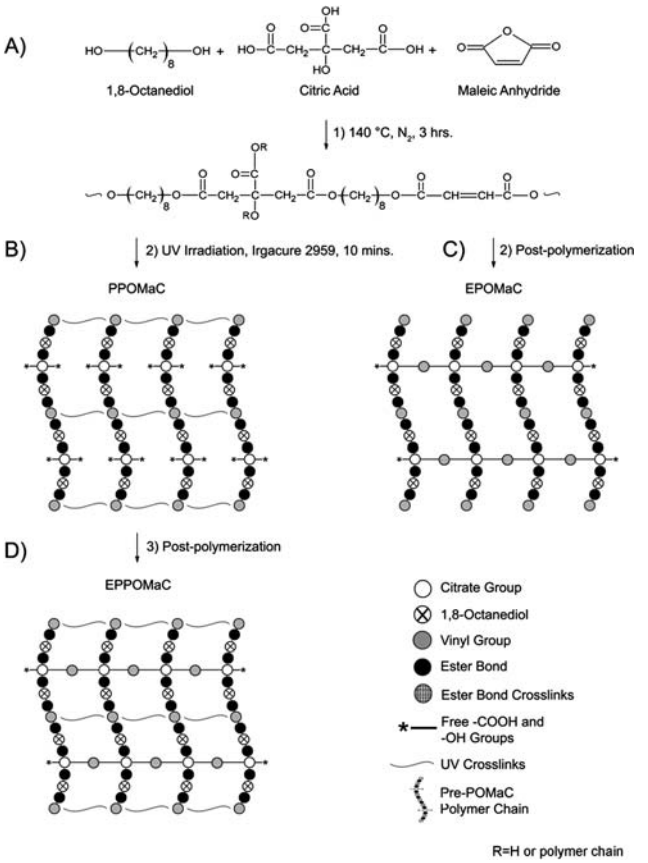

Fig. 1 A schematic representation of POMaC synthesis, networks, and dual crosslinking mechanism. (A) The monomers 1,8-octanediol, citric acid, and maleic anhydride underwent condensation polymerization to produce pre-POMaC with successful incorporation of vinyl carbons and degradable ester bonds located throughout the polymer backbone. (B) Upon exposure to UV irradiation, the free radical polymerization is initiated to crosslink pre-POMaC through the vinyl carrying carbons to yield photocrosslinked POMaC (PPOMaC). Notice the available free carboxylic acid and hydroxyl functional groups remaining from citric acid after photocrosslinking. (C) Pre-POMaC can also be crosslinked through polycondensation without photocrosslinking to obtain ester bond crosslinked POMaC (EPOMaC). (D) Post-polymerization can be used to further crosslink PPOMaC through the available free functional groups of citric acid to yield ester bond crosslinked photocrosslinked POMaC (EPPOMaC).

2 Experimental

Synthesis of Pre-POMaC

All chemicals were purchased from Sigma-Aldrich (St. Louis, MO), unless stated otherwise, and used as received. POMaC prepolymers were first synthesized by carrying out a controlled condensation reaction (Fig. 1A). Citric acid, maleic anhydride, and 1,8-octanediol were added to a 250 ml three-necked round bottom flask fitted with an inlet and outlet adapter. The mixture was melted under a flow of nitrogen gas by stirring at 160–165 °C in a silicon oil bath. The temperature of the system was subsequently lowered to 140 °C under a nitrogen purge and allowed to react for 3 h to create the POMaC pre-polymer. In order to remove any of the unreacted monomers and oligomers, the prepolymer was dissolved in 1,4-dioxane, and purified by drop wise precipitation in deionized water produced from a Direct-Q 5 Water Purification System (Millipore, Billerica, MA). The undissolved pre-polymer was collected and lyophilized in a Freezone 6 Freeze Dryer (Labconco, Kansas City, MO) to obtain the purified pre-POMaC.

Different pre-POMaC polymers were synthesized with different feeding ratios of citric acid to maleic anhydride (2 : 8, 4 : 6, and 6 : 4) to yield pre-POMaC 8, pre-POMaC 6, and pre-POMaC 4, respectively (Table 1). The ratio of the acids to the diol was kept as 1 : 1.

Pre-polymer characterization

^{1}H-NMR spectra for pre-POMaCs were recorded on a JNM ECS 300 (JOEL, Tokyo, Japan) at 300 MHz. The pre-polymers were purified twice as mentioned above and dissolved in dimethyl sulfoxide-d_6 (DMSO-d_6) (3 mg ml^{-1}). The chemical shifts in ppm for ^{1}H-NMR spectra were referenced relative to

Table 1 Feed ratios, actual molar composition, and molecular weight of POMaCs synthesized in this study

	Feed Ratio (mol)			Composition (mol)			
Polymer name	Maleic anhydride	Citric acid	1,8-Octanediol	Maleic anhydride	Citric acid	1,8-Octanediol	M_w (Da)
POMaC 4	2	3	5	1.94	3.26	4.90	624
POMaC 6	3	2	5	2.81	2.11	4.96	718
POMaC 8	4	1	5	3.77	1.12	4.92	945

tetramethylsilane (TMS, 0.00 ppm) as the internal reference. The average molecular weight of pre-POMaCs was characterized by matrix assisted laser desorption/ionization mass spectroscopy (MALDI-MS), which was done using an Autoflex MALDI-TOF Mass Spectrometer (Bruker Daltonics, Manning Park, MA). FT-IR spectra were obtained using a Nicolet 6700 FT-IR spectrometer (Thermo Fisher Scientific, Waltham, MA) at room temperature. Pre-POMaC samples were prepared by a solution-casting technique. A dilute solution of pre-POMaC in 1,4-dioxane (3 wt%) was cast onto a potassium bromide (KBr) crystal and allowed to dry for 12 h in a vacuum hood before being used to obtain the spectra.

Preparation and characterization of POMaC

In this study, three different POMaC networks were formed (Fig. 1). Photocrosslinked POMaC networks were formed by crosslinking through free radical polymerization. Pre-POMaC was dissolved in dimethylsulfoxide (DMSO) and mixed with photoinitiator (PI) 2-hydroxy-1-[4(hydroxyethoxy)phenyl]-2-methyl-1 propanone (Irgacure 2959) (1 wt%) to generate the free radicals. The pre-polymer solution was cast into a 38 mm diameter poly (tetrafluoroethylene) (PTFE) circular dish, and the polymerization reaction was initiated upon exposure to a 365 nm long wave ultraviolet light (UVP, Upland, CA) (Fig. 1B) at room temperature. The thermoset polymer achieved was then placed in an excess amount of DMSO to remove any unreacted polymer followed by immersion in deionized water to exchange the DMSO. The purified polymer was lyophilized to obtain photo-crosslinked POMaC (PPOMaC).

PPOMaC has the option to be further crosslinked *via* post-polymerization at 80 °C for pre-determined times to create ester bond crosslinked photocrosslinked POMaC (EPPOMaC) (Fig. 1D). POMaC networks, absent of any photocrosslinking, were also formed using a solution casting technique with 1,4-dioxane (30 wt%) as the solvent to assist in the fabrication of uniform films. 1,4-dioxane was chosen here because it can be easily evaporated to facilitate POMaC film formation before it is postpolymerized. The pre-polymer solution was cast into a PTFE circular dish, and allowed to dry overnight in a vacuum hood. The pre-polymer was then placed into an oven maintained at 80 °C for pre-determined times to crosslink the network (Fig. 1C). The thermoset polymer achieved was then placed in an excess amount of DMSO to remove any unreacted polymer followed by immersion in deionized water to exchange the DMSO. The purified polymer was lyophilized to obtain ester bond crosslinked POMaC (EPOMaC). FT-IR spectra were obtained for crosslinked PPOMaC and EPPOMaC films at room temperature. Pre-POMaC solutions were cast onto KBr crystals and crosslinked as mentioned previously to study the bond vibrations of the resulting crosslinked polymer network.

Tensile mechanical testing was conducted according to ASTM D412A on an MTS Insight 2 fitted with a 500 N load cell (MTS, Eden Prairie, MN). Briefly, the dog bone shaped samples (25 mm × 6 mm × 1.5 mm, length × width × thickness) were pulled at a rate of 500 mm min^{-1}, and elongated to failure. Values were converted to stress-strain and the initial modulus was calculated from the initial gradient of the curve (0–10% elongation). The results are presented as means ± standard deviation ($n = 6$). The density was measured by the fluid displacement method using a density measurement kit (Mettler Toledo, Columbus, OH). The auxiliary liquid used was deionized water. The crosslink density (η) and molecular weight between crosslinks (M_c) was calculated by eqn (1) according to the theory of rubber elasticity described elsewhere:[5]

$$\eta = \frac{E_0}{3RT} = \frac{\rho}{M_c} \quad (1)$$

where η represents the number of active network chain segments per unit volume (mol m^{-3}); M_c represents the molecular weight between crosslinks (g mol^{-1}); E_0 represents the initial modulus (Pa); R is the universal gas constant (8.3144 J mol^{-1} K); T is the absolute T (K); and ρ is the polymer density (g m^{-3}) as measured *via* the method above.

The sol content and swelling percentage was measured by the mass differential after incubation of the polymer network in DMSO. DMSO was chosen as the swelling agent due to its high boiling point. Briefly, polymer cylindrical discs (7 mm diameter; 2 mm thick) were cut from unpurified crosslinked films using a cork borer. The discs were weighed to find the initial mass (W_i), and suspended in DMSO for 72 h. The DMSO was changed every 24 h. The samples were removed from the DMSO, blotted dry with filter paper, and weighed (W_s). Next, the discs were suspended in deionized water for 24 h to exchange the DMSO, and lyophilized for 72 h. The dried samples, absent of any unreacted polymer, were weighed to find the dry mass (W_d). The sol gel fraction was calculated using the formula from eqn (2):[35]

$$\text{sol } (\%) = \frac{W_i - W_d}{W_i} \times 100 \quad (2)$$

The swelling percentage was calculated using the formula from eqn (3):[36]

$$\text{swelling } (\%) = \frac{W_s - W_d}{W_s} \times 100 \quad (3)$$

The reported values are the means ± standard deviation ($n = 6$). In addition to DMSO, swelling in water (37 °C) and phosphate buffered saline (PBS) (pH 7.4; 37 °C) were also performed using the same procedure.

In vitro degradation

Degradation studies were conducted in both PBS (pH 7.4) and NaOH solutions (0.05 M). NaOH degradation was used to screen the polymer degradation in a relatively short period of time.[6] Cylindrical disc specimens (7 mm in diameter; 2 mm thick) were cut from crosslinked, purified, and lyophilized films using a cork borer. The samples were weighed, placed in a tube containing PBS or NaOH (10 ml) for up to 10 weeks or 24 h respectively, and incubated at 37 °C. After incubation, samples were thoroughly washed with deionized water, lyophilized for 1 week, and weighed. The mass loss was calculated by comparing the initial mass (W_0) with the mass measured at the pre-determined time point (W_t), as shown in eqn (4).[37] The results are presented as the means ± standard deviation ($n = 6$).

$$\text{mass loss } (\%) = \frac{W_0 - W_t}{W_0} \times 100 \quad (4)$$

Microchannel scaffold fabrication

The microchannel pattern was transferred from polydimethylsiloxane (PDMS) molds to POMaC according to the procedures illustrated in Fig. 2. Briefly, pre-POMaC was dissolved in 1,4-dioxane to make a 30 wt% solution and mixed with PI (1 wt%). The pre-polymer solution was cast onto the PDMS microchannel mold, and placed under vacuum to remove any air trapped in the channels. The microchannels filled with pre-POMaC were then exposed to a UV irradiation for 10 min (Fig. 2A). Once the PPOMaC was formed in the microchannels, the particulate leaching method was used to fabricate porous POMaC scaffolds onto the microchannels. Pre-POMaC was dissolved in 1,4-dioxane to make a 30 wt% solution, followed by the addition of sieved sodium chloride salt (99% purity) with an average size in the range of 106–150 μm in a (1 : 9) polymer to salt ratio by weight. The polymer solution was mixed thoroughly with the salt and PI (1 wt%) until a viscous paste was formed. The resulting slurry was cast onto the previously fabricated PPOMaC microchannels. The scaffold was exposed to a 365 nm long wave ultraviolet light for 30 min.

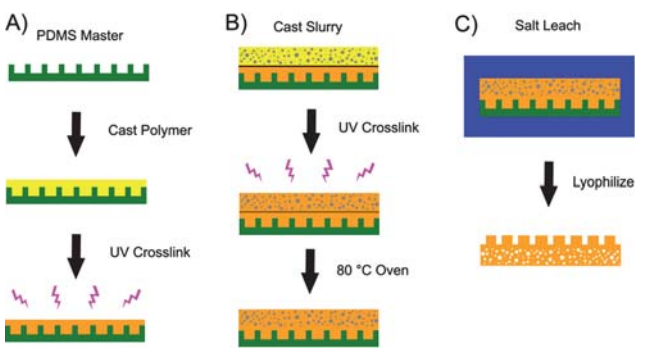

Fig. 2 (A) A schematic representation of the microchannel fabrication process: pre-POMaC, PI, and 1,4-dioxane are mixed together and cast over the PDMS master. Following the removal of air trapped in the channels, the pre-POMaC is exposed to UV irradiation to form PPOMaC channels. (B) A schematic representation of the scaffold addition process: pre-POMaC, PI, salt, and 1,4-dioxane are mixed together to create a thick slurry and cast over the PPOMaC channels. The slurry is then exposed to UV irradiation, and cured at 80 °C to fuse the scaffold to the microchannels. (C) Following post-polymerization, the entire scaffold/microchannel construct is suspended in deionized water to leach out the salt from the scaffold. The construct is then peeled away from the PDMS master and lyophilized to remove any water. The resulting scaffold is soft, flexible, and biodegradable with microchannels that can be used for cellular alignment (schematic not drawn to scale).

Following UV crosslinking, the entire scaffold/microchannel construct was placed in an oven and cured at 80 °C to ensure that the scaffold bonded to the PPOMaC microchannels (Fig. 2B). Next, the salt and any remaining solvent were leached out by immersion in deionized water for 72 h with water changes every 12 h. Finally, the scaffolds were lyophilized for 36 h to remove any traces of water. To view the cross-sectional morphology, the sample was freeze-fractured using liquid nitrogen, sputter coated with silver, and examined under a Hitachi S-3000N SEM (Hitachi, Pleasanton, CA). Image J analysis software was used to determine the channel widths and depths of the fabricated microchannels and scaffold pore sizes. To characterize the geometries, 3 random locations were selected and a total of 30 measurements performed. The dimensions reported are expressed as the means ± standard deviation.

In vitro cell attachment and proliferation

Cell compatibility for POMaC was evaluated *in vitro* using both qualitative and quantitative methods. EPPOMaC films and scaffolds were cut into cylindrical discs (7 mm in diameter) and sterilized in 70% ethanol for 3 h. After incubation in ethanol, the samples were exposed to UV light for 30 min and washed with PBS. NIH 3T3 fibroblasts (ATCC) were used as model cells for this study. The cells were cultured in Dulbecco's modified eagle's medium (DMEM), which had been supplemented with 10% fetal bovine serum (FBS) and 1% penicillin streptomycin. The culture flasks were kept in an incubator maintained at 37 °C, 5% CO_2, and 95% relative humidity. The cells were allowed to grow to the fourth passage, trypsinized, centrifuged, and suspended into media to obtain a seeding density of 1×10^5 cells ml^{-1} for both the films and scaffolds. Immediately prior to the trypsin treatment, 3T3 fibroblasts were labeled with carboxyfluorescein diacetate, succinimidyl ester (CFDA-SE) green fluorescent cell tracer using the manufacturer's protocol for the scaffold seeding. After 3 days of culture for the films, the cells were fixed with the addition of a 2.5% (wt/v) gluteraldehyde PBS solution. The fixed films were then sequentially dehydrated by treatment with a graded series of ethanol, lyophilized, and sputter coated with silver. The samples were then observed under SEM to view the morphology of the attached cells. In addition to the SEM images, separate samples were hematoxylin and eosin (H&E) stained, and viewed under a Zeiss Auxiovert inverted microscope (Carl Zeiss MicroImaging, Thornwood, NY). The seeded EPPOMaC scaffolds were allowed to culture, and imaged every other day for two weeks with re-staining on the third day. The scaffolds were removed from culture at day 2, 7, and 14 for fluorescent imaging of tracer dye stained cells. After imaging, the cell containing scaffolds were fixed in cold methanol for 10 min and dried under vacuum. Scaffolds were then embedded in a liquid gelatin-sucrose solution, placed under vacuum for 30 min, and frozen at −20 °C. Cross-sections of the scaffold were cut at 10 μm and

H&E stained to visualize cell penetration and growth throughout the scaffold.

A quantitative assessment of the cell proliferation on EPPOMaC scaffolds were also performed using a methylthiazoletetrazolium (MTT) cell proliferation and viability assay kit. EPPOMaC scaffolds were cut into cylindrical discs (7 mm in diameter), and sterilized as mentioned above. PLLA scaffolds were used as a relative control. 3T3 fibroblasts were seeded on the scaffolds in the same manner as mentioned previously. MTT Assay analysis was performed at 1, 3, and 7 days of culture. At the pre-determined time point, the assay was performed as per the manufacturer's protocol.

Briefly, the old media was aspirated, and each sample was washed with PBS to remove any loosely attached or dead cells. Next, incomplete media (100 μl) (absent of any FBS) was added to the specimens. 3-(4,5-dimethylthiazol-2yl)-diphenyltetrazolium bromide solution (10 μl) was then added to the samples, and allowed to incubate for 3 h. At the end of the incubation period, the mixture of the MTT solution and incomplete media was aspirated and replaced with MTT solvent (100 μl). Dissolution of the formazan crystals was facilitated by constant agitation of the well plate on an orbital shaker for 20 min. The absorbance was measured with an Infinite200 microplate reader (Teacan Group Ltd., Switzerland) at 570 nm, with a reference wavelength of 690 nm, within 30 min of MTT solvent addition.

Foreign body response

PPOMaC, EPPOMaC, and PLLA (as relative control) were used to evaluate the *in vivo* response. The films were cut into discs (7 mm diameter; 1 mm thickness), and sterilized under UV light for 30 min per side and soaked in 70% ethanol. The films were then exchanged with PBS to remove the ethanol and dried under vacuum for 30 min. The sterilized films were then implanted subcutaneously in the back of healthy Balb/C mice (The Jackson Laboratories, Bar Harbor, ME). Animals were cared for in compliance with regulations of the animal care and use committee of University of Texas at Arlington. 12 mice were divided into three groups of four (2 male and 2 female) for the different time points of the study. The mice were anesthetized in a chamber through which an isofluorane-oxygen mixture was passed. Test samples were randomly implanted in upper or lower part of the back of the mice by blunt dissection. The mice were monitored through recovery from anesthesia and placed into single housing and monitored throughout the study. At the end of each time point, the mice were sacrificed by CO_2 inhalation, and the implant and surrounding tissue were frozen in OCT embedding media (Polysciences Inc., Warrington, PA) at −80 °C for histological analyses.

To assess the tissue responses to the implants, 10 μm tissue sections were H&E stained. Images of stained sections were taken at 10 × magnifications using a Leica DMLP microscope (Leica Microsystems Inc., Bannockburn, IL) fitted with a Nikon E500 camera (Nikon Corp., Japan). Three images per section were collected from different parts of the section for analysis. A total of four sections per animal were examined in this manner. Response capsule thickness was measured in each of the images using Image J analysis software. At least 25 readings from different parts of the images were collected and averaged to determine the capsule thickness. Immunohistochemical stains were performed to determine inflammatory cell engraftment for biomaterial implants. Inflammatory cells were identified by CD11b positive expression.[38] All of the primary and second antibodies used in this work were purchased from Santa Cruz Biotech (Santa Cruz, CA). Stained sections were visualized using a Leica microscope and imaged with a CCD camera (Retiga EXi, Qimaging, Surrey BC, Canada).

Statistical methods

Data are expressed as means ± standard deviation. The statistical significance between two sets of data was calculated using a two-tail Student's t-test. Non-parametric one-way ANOVA tests were also performed where appropriate. Data were taken to be significant, when $p<0.05$ was obtained.

3 Results

3.1 Pre-POMaC synthesis and characterization

All the pre-polymers were prepared through an initial polycondensation reaction between citric acid, maleic anhydride, and 1,8-octanediol (Fig. 1A). The stoichiometric ratios prepared in this study are shown in Table 1. The average molecular weight (M_w) of the pre-POMaC polymers was 624, 718, and 945 Da for pre-POMaC 4, pre-POMaC 6, and pre-POMaC 8, respectively, as determined by MALDI-MS. All POMaC pre-polymers consisted of a transparent viscous liquid at room temperature after the initial polycondensation reaction. Pre-POMaCs were found to be soluble in most organic solvents such as 1,4-dioxane, DMSO, dimethylformamide (DMF), tetrahydrofuran (THF), and acetone.

FT-IR analysis confirmed the presence of various functional groups in the polyester based pre-polymer. The peak located at 1647 cm^{-1} validated the successful incorporation of the vinyl group contributed by the maleic anhydride (Fig. 3A). Furthermore, the peaks located at 1720 and 3570 cm^{-1} confirmed the preservation of pendant carboxylic acid and hydroxyl groups, respectively. The broad peaks centered at 2932 cm^{-1} were assigned to methylene groups contributed by both 1,8-octanediol and citric acid.

The resonance of various hydrogens in the pre-polymer backbone was confirmed by analyzing the chemical shifts of the ^{1}H-NMR peaks with respect to tetramethylsilane (TMS). Fig. 3B shows a typical ^{1}H-NMR spectrum of a pre-POMaC. The peaks located between 6 and 7 ppm (a) were assigned to the protons in –C*H*=C*H*– incorporated into the polymer chain. The peaks (b) located at 2.79 ppm were assigned to –CH_2– from citric acid. The peaks (d) located at 1.53 ppm were assigned to in –O–CH_2CH_2– from 1,8-octanediol.[6,39] The chemical compositions of the pre-polymers were determined by calculating the ratios of the signal intensities of the characteristic proton peaks from each monomer: maleic anhydride (a/2), citric acid (b/4), and diol (d/4). As shown in Table 1, the actual polymer composition can be well controlled by varying the feeding ratio of the monomers in the initial polycondensation.

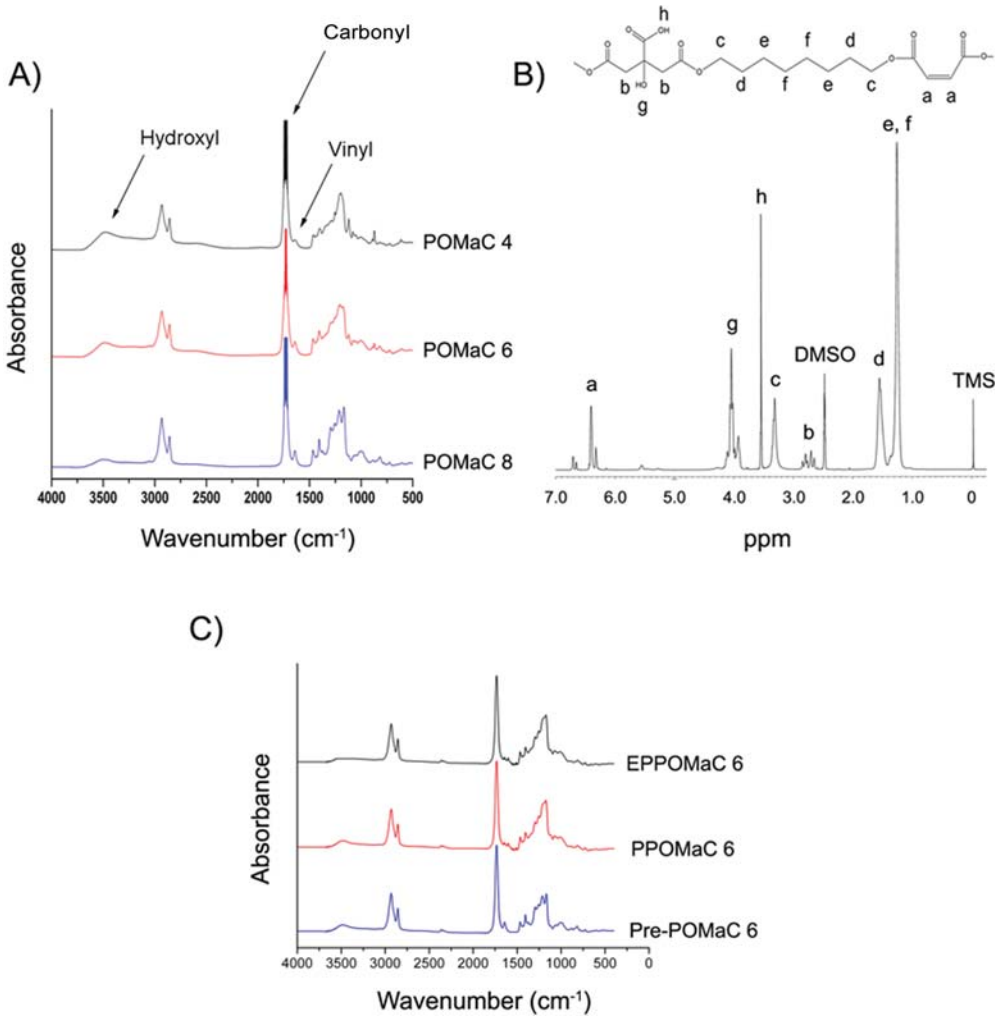

Fig. 3 Structural characterization of POMaC networks. (A) FT-IR spectra of POMaC pre-polymers. (B) ^{1}H-NMR spectra of pre-POMaC 8. (C) FT-IR spectra of crosslinked POMaC films.

3.2 Preparation and characterization of POMaC

Three different networks using two different modes of crosslinking were utilized to polymerize pre-POMaCs into a thermoset polyester elastomer as summarized in Fig. 1: free radical polymerization, ester bond crosslinking, and a combination of both free radical polymerization followed by ester bond polymerization. The former crosslinking mechanism utilized the vinyl groups present in the pre-polymer, which can be directly polymerized into a hydrogel like material within 10 min (Fig. 1B). FT-IR analysis on UV crosslinked films shows a significant reduction of the peak located at 1647 cm^{-1}, which was designated to the vinyl group from maleic anhydride. Whereas ester bond crosslinks were formed through post-polycondensation of the citric acid pendant carboxylic and hydroxyl groups in the presence of heat (Fig. 1C). Furthermore, both crosslinking mechanisms can be combined in order to produce a higher crosslinked network as needed for a particular application (Fig. 1D). When the pre-polymer was crosslinked *via* ester bond formation, a significant reduction in the hydroxyl peak located at 3570 cm^{-1} was evident (Fig. 3C).

The mechanical properties of POMaC networks are summarized in Table 2. A significant reduction in the initial modulus (0.29 to 0.04 MPa) and peak stress (611 to 245 kPa) was exhibited as the molar concentration of the maleic anhydride was reduced from 8 to 4, respectively. However, the elongation at break increased (194 to 441%) when the maleic anhydride ratio was reduced in the same manner. The crosslinking density of photopolymerized POMaC films also decreased (39.78 ± 4.76 to 5.48 ± 1.38 mol m^{-3}) as the molar ratio of the maleic anhydride was reduced from 8 to 4, respectively. The relative molecular mass between crosslinks of the PPOMaC films was shown to be inversely proportional to the density of the crosslinks within the polymer network.

The mechanical properties of POMaCs were also tuned through the DCM. Table 3 shows the mechanical properties of POMaCs crosslinked using photopolymerization and/or ester bond crosslinking. When photopolymerization was avoided, in the case of EPOMaCs, a peak stress of 326.32 ± 85.46 kPa, initial modulus of 0.12 ± 0.02 MPa, and elongation at break of $327 \pm 56\%$ was observed when crosslinked at 80 °C without vacuum for

Table 2 Density measurements, mechanical properties, and crosslinking characterization of photocrosslinked POMaC networks with different ratios of maleic anhydride. PPOMaCs were crosslinked under UV irradiation for 10 min, 30% polymer concentration, and 1 (wt%) PI[a]

Sample	Density (g cm^{-3})	Peak stress (kPa)	Young's modulus (MPa)	Elongation (%)	η (mol m^{-3})	M_c (g mol^{-1})
PPOMaC 4	1.08 {0.01}	245 {41.29}	0.04 {0.01}	441 {93}	5.48 {1.38}	206098 {45482}
PPOMaC 6	1.09 {0.01}	319 {74.58}	0.08 {0.01}	360 {20}	10.56 {0.66}	104208 {6799}
PPOMaC 8	1.11 {0.02}	611 {24.48}	0.29 {0.04}	194 {10}	39.78 {4.76}	28560 {4098}

[a] Values are reported as the mean followed by the standard deviation in braces.

Table 3 Density measurements, mechanical properties, and crosslinking characterization of photocrosslinked and ester bond crosslinked POMaC networks. EPOMaCs were post-polymerized at 80 °C for the corresponding number of days in parenthesis. EPPOMaC polymers were crosslinked under UV irradiation for 10 min, 30% polymer concentration, 1 (wt%) PI, and post-polymerized at 80 °C for the corresponding number of days in parenthesis[a]

Sample	Density (g cm^{-3})	Peak stress (kPa)	Young's modulus (MPa)	Elongation (%)	η (mol m^{-3})	M_c (g mol^{-1})
EPOMaC 6 (1 day)	1.13 {0.01}	326.32 {85.46}	0.12 {0.02}	327 {56}	15.79 {2.58}	73287 {12109}
EPOMaC 6 (2 days)	1.16 {0.01}	781.16 {60.04}	1.36 {0.16}	90 {6}	185.63 {22.15}	6351 {748}
EPPOMaC 6 (1 day)	1.17 {0.01}	503.64 {50.30}	0.25 {0.01}	269 {22}	34.71 {1.77}	33776 {1699}
EPPOMaC 6 (2 days)	1.17 {0.01}	994.14 {38.00}	1.52 {0.02}	51 {3}	206.92 {3.28}	5655 {89}

[a] Values are reported as the mean followed by the standard deviation in braces.

a 1 day time period. There was a significant increase in the peak stress (781.16 ± 60.04 kPa) and initial modulus (1.36 ± 0.16 MPa), but a decrease in elongation at break (90 ± 6%) when the post-polymerization time was lengthened to 2 days ($p<0.05$). A similar trend in mechanical properties was reported for the previously published elastomer poly(diol citrates).[28]

When photocrosslinking and ester bond crosslinking was combined as the mode of polymerization in EPPOMaC, there was a significant increase in the peak stress, initial modulus, and reduction in elongation at break for both EPPOMaC 6 (1 day) (503.64 ± 50.30 kPa, 0.25 ± 0.01 MPa, and 269 ± 22%) and EPPOMaC 6 (2 days) (994.14 ± 38 kPa, 1.52 ± 0.02 MPa, and 51 ± 3%), respectively. The mass densities of POMaC networks ranged from 1.08 to 1.17 g cm^{-3} and were dependent upon the composition and crosslinking method used. The crosslinking densities of both EPOMaCs and EPPOMaCs showed an increase when the post-polymerization time was increased from 1 to 2 days (15.79 ± 2.58 to 185.63 ± 22.15 and 34.71 ± 1.77 to 206.92 ± 3.28 mol m^{-3}), respectively.

The sol content of PPOMaC networks varied between 52 and 18% by mass, and was reduced by increasing the maleic anhydride ratio, polymer concentration while crosslinking, and photoinitiator concentration (data not shown). POMaC networks exhibited a solvent uptake, which varied from 146 to 2265% by mass across composition and crosslinking conditions. The percentage of swelling was inversely related to the amount of maleic anhydride in the polymer network. As seen in Fig. 4A, the swelling percentage decreased from 2143.12 ± 121.90% to 1344.19 ± 84.66% as the ratio of the maleic anhydride increased from 4 to 8. A similar trend was observed when PBS was used as the swelling agent (1011.23 ± 137.23 to 276.55 ± 11.32%).

The swelling characteristics of the polymer networks were also evaluated on POMaCs using different modes of crosslinking. As shown in Fig. 4B, there was a significant reduction in swelling properties with all three swelling agents when the ester bond crosslinking time was increased from 1 to 2 days ($p<0.05$). For example, EPOMaC 6 (1 day) exhibited a solvent uptake of 510.57 ± 23.54%, whereas EPOMaC 6 (2 days) swelled only 298.80 ±

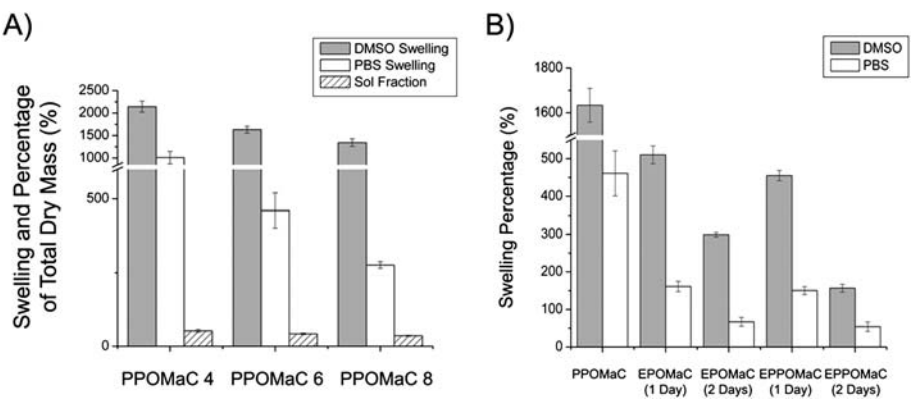

Fig. 4 (A) Degree of swelling and sol content as a function of the ratio of maleic anhydride in pre-POMaC. PPOMaC networks were crosslinked with 10 min UV irradiation, 30% polymer concentration, and 1 (wt%) PI. (B) Degree of swelling in solvent and PBS as a function of the dual crosslinking mechanism.

62.39%. The same decrease in swelling was observed for EPPOMaCs, and when PBS was used as the swelling agent for the DCM. Interestingly, a significant difference in the solvent uptake between EPOMaC and EPPOMaC was seen ($p<0.05$), but no significant difference was observed when PBS was used as the swelling agent ($p>0.05$).

3.3 *In vitro* degradation

In addition to degradation in PBS, accelerated degradation studies were performed to ensure that the material's hydrolytically liable bonds were accessible and that the degradation products are completely soluble. Complete degradation of all POMaC polymers were confirmed by degradation in the presence of 0.05 M NaOH. The data for the degradation characterization of POMaC networks are presented in Fig. 5. The degradation rate of the polymer could be adjusted by varying the molar ratio of the maleic anhydride, and through the DCM. PPOMaC polymers with higher maleic anhydride ratios resulted in slower degradation rates. The additional crosslinking through ester bond formation also resulted in longer degradation rates. PPOMaC 4 was shown to have degraded 77.50 ± 1.93%, whereas EPPOMaC 8 (2 days) degraded only 18.45 ± 4.44% by week 10 in PBS.

3.4 Microchannel scaffold fabrication

The microchannels and microchannel scaffold (Fig. 6) demonstrate the processability of POMaCs. The surface topology of the micropatterned PPOMaCs created by a replica molding technique was verified using SEM. Fig. 6A and 6B show that the fabricated microchannels resulted in column and channel widths of 210.77 ± 0.82 and 78.24 ± 0.84 μm, respectively. The SEM images of PPOMaC microchannel cross-sections show that the depth of each channel was 131.53 ± 1.66 μm as seen in Fig. 6C. The microchannel scaffold construct produced pore sizes ranging from 106–150 μm in size with interconnectivity as seen in Fig. 6D. All POMaC scaffolds were soft and could recover from bending deformations.

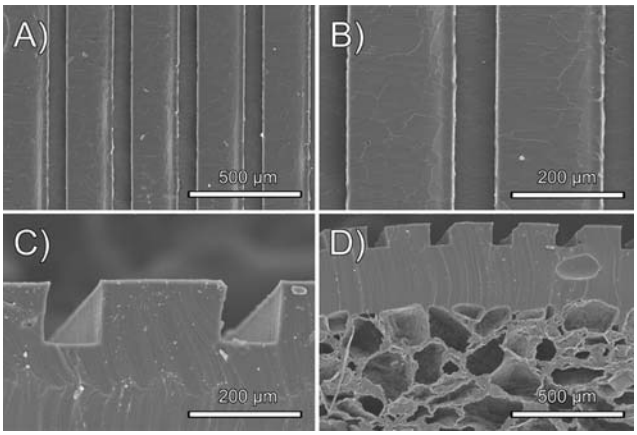

Fig. 6 Representative SEM images of the PPOMaC microchannel negatives produced from PDMS molds. A, B, and C show the characterization of the replica-molded PPOMaC substrate. (D) Cross-section of EPPOMaC salt leached scaffold (salt size 150–250 μm) bonded to EPPOMaC channels.

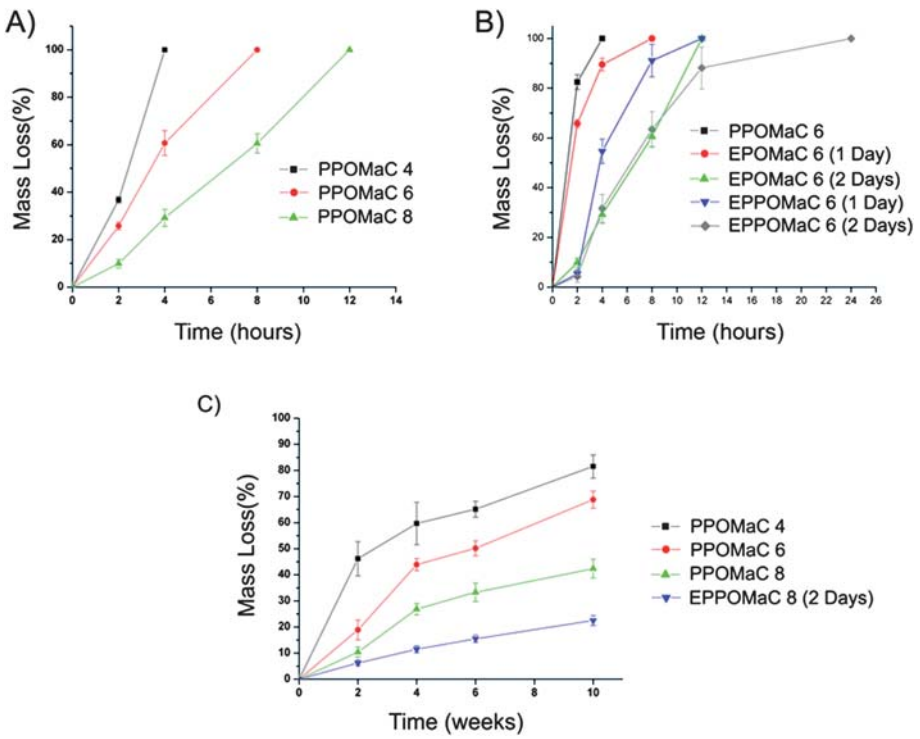

Fig. 5 (A) *In vitro* degradation in 0.05 M NaOH as a function of the ratio of maleic anhydride in pre-POMaC. PPOMaC networks were crosslinked with 10 min UV irradiation, 30% polymer concentration, and 1 (wt%) PI. (B) *In vitro* degradation in 0.05 M NaOH as a function of the dual crosslinking mechanism. (C) *In vitro* degradation of POMaC networks in PBS (pH 7.4; 37 °C).

3.5 *In vitro* cell attachment and proliferation

Cell adhesion of POMaCs was observed 72 h after cell seeding. As shown in Fig. 7A and 7B, 3T3 fibroblasts cultured on EPPOMaC films attached and displayed a normal morphology. Cell adhesion and proliferation were quantitatively evaluated on EPPOMaC and PLLA porous scaffolds using a MTT assay (Fig. 7C). The results indicated that the cell adhesion and proliferation were initially higher on the PLLA scaffolds (day 1 and 3). However, EPPOMaC scaffolds showed a higher rate of cell proliferation and were almost comparable to the PLLA cell numbers by day 7 ($p>0.05$).

Fig. 8 shows the behavior of CFDA-SE labeled 3T3 fibroblasts seeded onto EPPOMaC scaffolds monitored over 2 weeks. Initially, a light density of cells accumulated along the scaffold surface (day 2). By day 7, the cell proliferation and density increased along the scaffold surface as seen by the dense cell clusters. After 14 days, the cells continued to proliferate along the exterior and started to migrate into the interior of the scaffold. H&E photomicrographs of 3T3 fibroblasts cultured up to two weeks show that cells were able to colonize on POMaC scaffolds. EPPOMaC scaffold cross-sections at 1 and 2 weeks of cell culture are shown in Fig. 9. At 1 week, cells are found scattered in dense groups on the scaffold surface. By week 2, thick bands of 3T3 fibroblasts were observed growing along the outside of the scaffold along with increased infiltration of cells through the porous scaffold network.

3.6 *In vivo* host response evaluation

The foreign body response of PPOMaC and EPPOMaC was evaluated *via* subcutaneous implantation in mice. Fig. 10 shows

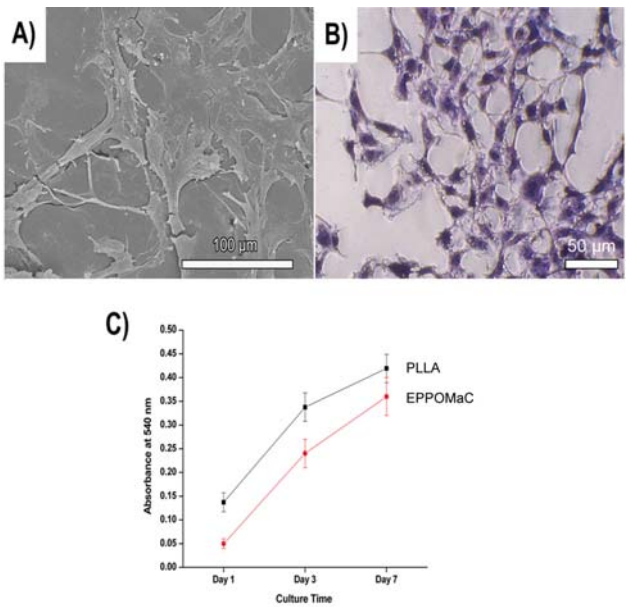

Fig. 7 (A) Representative SEM image of NIH 3T3 fibroblast spreading after 72 h of culture on EPPOMaC. (B) Representative photomicrograph of the H&E stained cell monolayer after 72 h of culture on EPPOMaC. (C) Comparison of 3T3 fibroblast growth and proliferation on PLLA (relative control) and EPPOMaC scaffolds. MTT absorption was measured at 570 nm ($n = 6$).

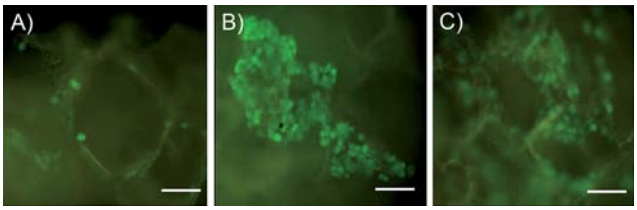

Fig. 8 The behavior of CFDA-SE labeled 3T3 fibroblasts seeded onto EPPOMaC scaffolds. (A) Initially, a light density of cells located along the scaffold surface could be seen (day 2). (B) By day 7, the cell density elevated as evident by dense cell clusters located on the scaffold surface. (C) After 14 days, the cells could be observed growing along the edge of surface pores and had migrated into the interior of the scaffold (scale bar = 50 μm).

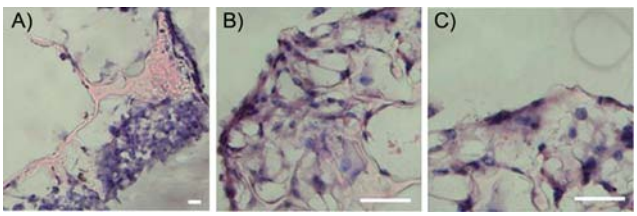

Fig. 9 Photomicrographs of EPPOMaC scaffold cross-sections at 1 and 2 weeks of cell culture. (A) At 1 week, cells are found scattered in dense groups on the scaffold surface. (B) By week 2, thick bands of 3T3 fibroblasts are observed growing along the outside of the scaffold. (C) Interior scaffold cross-sections show increased infiltration of cells through the porous scaffold network (scale bar = 50 μm).

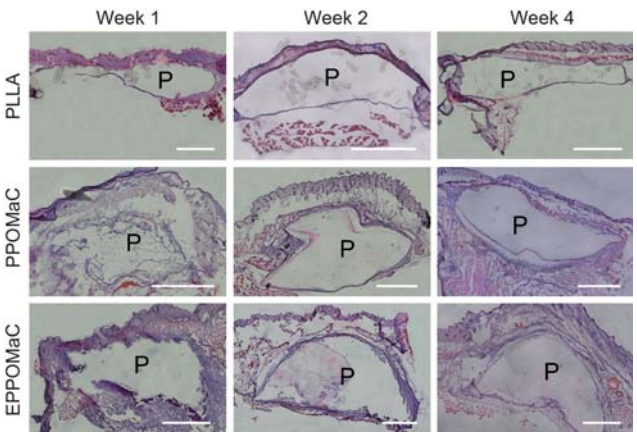

Fig. 10 Representative images of H&E stained sections demonstrating the foreign body response of PLLA (control), PPOMaC, and EPPOMaC films implanted subcutaneously in Balb/C mice. Images are at 10× and scale bar represents 1 mm. "P" represents polymer section.

photomicrographs of H&E stained cross-sections of PPOMaC and EPPOMaC implants and the surrounding tissues. Given that biomaterial implants elicit varying degrees of tissue responses, the thickness of inflammatory cell infiltrate was quantified. This thickness was correlated to estimate the degree of inflammatory cell response (Fig. 11). PLLA films were implanted and characterized as a model biomaterial implant. Consistent with many prior observations, PLLA films initiated inflammatory cell accumulation at week 1 (~100 μm), which gradually decreased

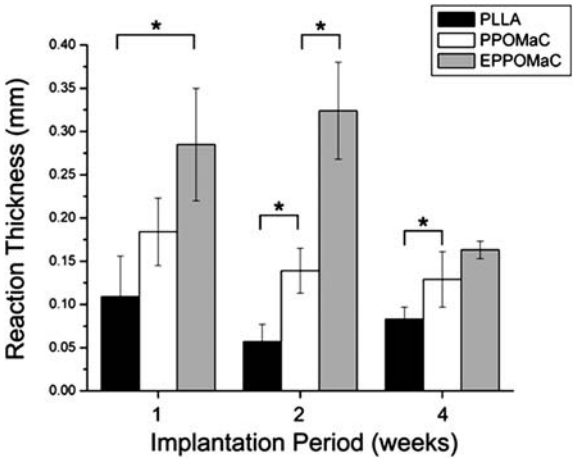

Fig. 11 Characterization of the foreign body response to PLLA, PPOMaC, and EPPOMaC implants. The response thickness was found to be larger for EPPOMaC films when compared to PLLA at all time points, but was significantly reduced by 4 weeks. The response thickness of PPOMaC implants decreased throughout the implantation period and was found to be comparable to the PLLA implants.

into week 2 (~50 μm) and week 4 (~75 μm) consistent with a decrease in cells of leukocyte morphology and an increase in cells of fibroblast morphology.

Interestingly, PPOMaC and EPPOMaC displayed different degrees of inflammatory cell responses. EPPOMaC generated a more pronounced response than PPOMaC at each time point investigated. Similar to the PLLA response, PPOMaC had an accumulation of cells around the implant at week 1 (175 μm), which showed a decreasing trend at weeks 2 and 4 (both ~125 μm). However, the EPPOMaC film generated an increased number of encapsulating cells at both week 1 (1.5 × PPOMaC) and week 2 (3 × PPOMaC), significantly higher than both PLLA and PPOMaC ($p>0.05$). After 4 weeks of implantation, the response thickness for both PPOMaC and EPPOMaC significantly decreased by 30% (184 ± 39 to 129 ± 32 μm) and 43% (285 ± 65 to 163 ± 10 μm), respectively.

To further characterize the foreign body response, the CD11b expression in the cell-encapsulating layer at week 2 was examined as a measure of the neutrophil and monocyte/macrophage responses. This time point was chosen based on tissue responses to the polymer films, which exhibited the greatest difference in cell accumulation at week 2. In all implant groups, a mutli-cell layer staining positive for CD11b was seen. PLLA (Fig. 12A) had a layer of $CD11b^+$ of only a few cells in thickness, while both PPOMaC (Fig. 12B) and EPPOMaC (Fig. 12C) had a more pronounced, multi-cell thick response. Interestingly, the density of these cells inside the infiltrate layers is similar among all groups (Fig. 13A). However, when the thickness of the $CD11b^+$ cell layer between groups was quantified (Fig. 13B), a significant difference in the degree of the response was observed. Similar to measurements of thickness for the total cell layer, we find the $CD11b^+$ cell response decreases from EPPOMaC > PPOMaC ≥ PLLA.

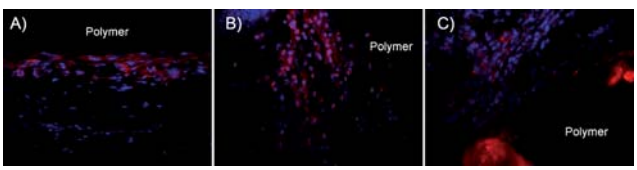

Fig. 12 Representative images of CD11b stained sections demonstrating the foreign body response of (A) PLLA (control), (B) PPOMaC, and (C) EPPOMaC films implanted subcutaneously in Balb/C mice after 2 weeks.

4 Discussion

The purpose of this study was to synthesize and evaluate a new biodegradable elastic platform biomaterial that is able to fine-tune the material properties of the resulting material through a DCM. The basic components of POMaC were based upon the previously reported biodegradable elastomer, poly(diol citrates) POC, which has shown excellent biocompatibility both *in vitro* and *in vivo*.[6] By combining the advantages of free radical polymerization and ester bond crosslinking, a new class of polyester elastomers has been created with the ability to be crosslinked into a three-dimensional network using a combination of two different mechanisms. Thus, the rapid crosslinking of the network into a hydrogel is possible, and additional degradable ester crosslinks can be introduced throughout the polymer

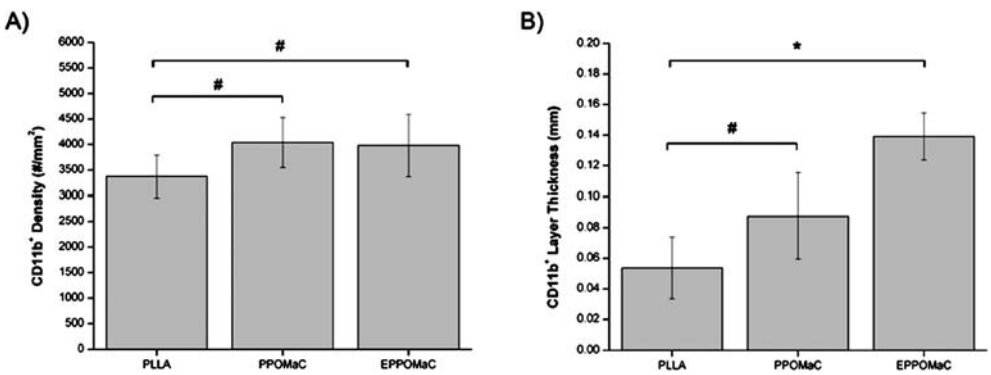

Fig. 13 Characterization of the $CD11b^+$ foreign body response to PLLA, PPOMaC, and EPPOMaC implants after 2 weeks. $CD11b^+$ cell density was found to be similar for all polymer groups. EPOMaC films displayed a significant difference in $CD11b^+$ thickness, whereas PPOMaC films were found to be comparable to PLLA.

network to enhance the mechanical properties without compromising the degradation capability.

The materials synthesized in this study cover a wide range of swelling ratios, mechanical properties, degradation profiles, and functionalities, which are important in controlling the biological response to an implanted material.[15] The free functional groups available after free radical polymerization are useful moieties for the potential modification of the material with proteins or peptides to activate a desired cellular response.[40] Unlike other materials, POMaCs offers an additional advantage in that extra treatment to create these chemical moieties is not needed.[41,42]

The synthesis of pre-POMaCs, which is conducted through a controlled polycondensation reaction between maleic anhydride, citric acid, and 1,8-octanediol, is simple and cost-effective. The melting polymerization provides an easy way to scale up the biomaterial preparation.[43] POMaCs are inexpensive to produce, easy to synthesize, and are adaptable to most polymer processing capabilities.[44] The reaction was driven forward by the removal of water through the addition of heat to produce a random copolymer with degradable ester bonds throughout the polymer backbone. Maleic anhydride was chosen as a means to incorporate a vinyl group into the pre-POMaC backbone in order to crosslink the polymer network through free radical polymerization. Citric acid was chosen as a multifunctional monomer, which contributed pendant carboxylic acid and hydroxyl groups in the pre-polymer backbone for the future incorporation of specific factors, and the option for further post-polymerization. The polycondensation reaction yielded a low molecular weight, low viscosity pre-polymer, which gives POMaC the option to be used without a solvent system for *in situ* applications.

Pre-polymer FT-IR analysis (Fig. 3C) shows the successful incorporation of the vinyl group and preservation of the carboxylic and hydroxyl functionalities in all pre-POMaC polymers. As the molar ratio of the maleic anhydride is decreased, the ratio of the vinyl group peak to the hydroxyl group peak was reduced, which is also supported in the ^{1}H-NMR evaluation. The reduction of the double bond peak located at 1647 cm^{-1} in the photocrosslinked films verified the consumption of the vinyl group during the free radical polymerization, and the preservation of the broad peak located at 3750 cm^{-1} confirmed the presence of the unreacted pendant functional groups, which were partially consumed in the oven crosslinked films.

The chemical compositions determined from ^{1}H-NMR were consistent with the feed ratios to show that the molar ratios can be precisely controlled during synthesis (Table 1). The two pairs of vinyl hydrogen peaks located between 6 and 7 ppm were contributed by maleic anhydride vinyl groups located in the middle and at the end of the polymer chain.[39] Decreasing the maleic anhydride ratio during the pre-polymer synthesis resulted in networks with increased functionalities, which was confirmed by an increase in the area of the hydroxyl proton peaks. Thus, the functionalities in the pre-polymer can be easily modulated towards a specific application, which is an important parameter in the outcome of the material properties for POMaCs.

In the case of photocrosslinked films, the swelling capability of the polymer was directly correlated to the amount of maleic anhydride in the polymer. As shown in Fig. 4A, the total uptake ability of the polymer was significantly lowered for all swelling agents as the amount of maleic anhydride was increased. This is due to the fact that the vinyl functionality contributed by the maleic anhydride was solely responsible for the crosslinking of the network in the free radical polymerization. This was supported by the calculated values of the crosslinking density where the increased amount of maleic anhydride in the polymer resulted in a higher number of crosslinks in the network. In addition, a decrease in the maleic anhydride corresponded to an increase in the citric acid, which contained carbonyl and hydroxyl chemistries to increase the hydrophilicity of the polymer. Thus, swelling for the polymer with a higher molar ratio of maleic anhydride was restricted. These findings were confirmed by the degradation characteristics of the polymer. The degradation rate for POMaC polymers was controlled through the hydrophilicity and crosslinking density of the resulting network. Thus, increasing the citric acid content and lowering the crosslinking degree created a polymer with a faster degradation rate.

Engineering soft and elastic tissues such as lung tissue (5–30 kPa), skeletal muscle (100 kPa), and cardiac muscle (20–150 kPa) have sparked the development of soft biodegradable elastomers.[45] It has been recognized that the mechanical properties of tissue-engineered scaffolds potentially have an influence on the inflammatory response, angiogenesis, and wound healing process.[46] In addition, previous research has shown that soft and elastic scaffolds are more conducive to angiogenesis when compared to stiffer scaffolds.[4] Therefore, it is important to closely match the mechanical properties of scaffolds with the targeting tissues for tissue engineering. The reported mechanical properties of POMaCs cover most of the above soft tissues. POMaCs are unique in that the mechanical properties of polymer networks can be fine tuned by adjusting monomer ratios and balancing the carbon-carbon crosslinking with ester bond crosslinking. Unlike other reported biodegradable elastomers, in which increasing the crosslinking degree to obtain higher mechanical strength results in the loss of valuable pendant functional groups, the DCM mechanism will allow for a more flexible design.[6,28]

For example, decreasing the maleic anhydride amount in the polymer backbone resulted in a very soft and elastic polymer when crosslinked only through the free radical polymerization. Adjusting the free radical crosslinking degree may adjust material properties without sacrificing pendant functional groups. An additional control over the ester bond crosslinking may increase the stiffness and strength of the polymers if needed. Thus, there is a fine balance between the amount of maleic anhydride and citric acid along with the DCM in order to achieve the proper material properties for the target application.

The preliminary *in vitro* and *in vivo* biocompatibility evaluations of POMaC confirm their potential as a suitable biomaterial. *In vitro* results of cell adhesion and proliferation demonstrate good cell-material interaction. 3T3 fibroblasts seeded onto POMaC films were viable and displayed a normal morphology. However, quantitative analysis from MTT assay showed that cells did not initially proliferate as well as PLLA, but did display a similar growth pattern. Unlike many other hydrogels which require pre-treatment with adhesion peptides or proteins for cell culture, the *in vitro* cell attachment and proliferation on POMaCs were performed without any pre-treatment.[35,47] Furthermore, POMaCs offer room for improvement through the available pendant groups available for the conjugation of proteins or other cell specific factors if needed.

Several recent papers have used the thickness of the cellular infiltrate around the biomaterial to assess the degree of tissue response.[48–50] This buildup of inflammatory cells and fibroblasts initiates the formation of granulation tissue and fibrotic capsule surrounding biomaterial implants. PLLA films were chosen as a model comparison to PPOMaC implants due to their ubiquitous use in biomedical applications. The degree of *in vivo* cell encapsulation to PPOMaC implants is similar to previously published reports using biodegradable elastomers assessed over the first 4 weeks of implantation.[28,50] In addition, the nature of this response appears related to the crosslinking methods used to create the material, as the PPOMaC films had a substantially decreased response at weeks 1 and 2 compared to EPPOMaC films. Beyond the cell accumulation around the implants, the nature of the neutrophil and macrophage responses was investigated, as the degree of activation of these adherent cell types to the biomaterial can dictate fibroblast interactions and fuel fibrotic encapsulation.[51,52]

Using the responses to PLLA films as comparison, PPOMaC accumulated only slightly more $CD11b^+$ cells around film implants, suggesting a similar degree of response and activation to PLLA. A similar crosslinking effect was observed for EPPOMaC, as these films appear to accumulate substantially more $CD11b^+$ cells than PPOMaC films. This can perhaps be explained by the difference in material physical properties, with the higher modulus EPPOMaC films potentially causing more mechanical agitation in the subcutaneous implantation model over the course of the 2-week implantation period. In addition, PPOMaC networks exhibit more hydrogel like properties, which have been shown to be very biocompatible due to their mechanical compliance and mass transfer properties.[18] A more thorough analysis of the inflammatory cell response and long-term fibrotic response is needed to validate whether the tissue response to these materials is indeed comparable.

The combination of elastomers with micro-electro-mechanical systems (MEMS) technologies has sparked a new area of research with increasing practical applications.[53] The capability to specifically control the size and shape of biologically relevant materials has provided new opportunities in addressing some of the challenges in tissue engineering such as vascularization, tissue architecture, tissue organization, and cell seeding.[54] POMaC has demonstrated versatile processability and the ability to be fabricated into complex geometries as shown by the microchannel scaffold (Fig. 6D). By using a soft lithographic approach, replica-molded POMaC constructs were created for future research in developing vasculature and organized tissues in contact guidance applications.

5 Conclusion

We have developed a new class of novel elastomeric biomaterials that are synthesized using inexpensive monomers and a cost-effective synthesis procedure. The application of POMaC is not limited to any single application in that the DCM allows for the option of crosslinking the material through UV irradiation and/or polycondensation. POMaCs exhibit a wide range of material properties that can be controlled using the dual crosslinking mechanism. The softness of the material can be fine tuned to meet the requirements for soft tissue engineering applications. The development of POMaC and the dual crosslinking mechanism should contribute to the biomaterials science.

Acknowledgements

This work was supported in part by American Heart Association Beginning Grant-in-Aid award (to J.Y.), award R21EB009795 from the National Institute of Biomedical Imaging and Bioengineering (NIBIB) (to J.Y.) and NIH R01 GM074021 (to L.T).

Notes and references

1 A. R. Webb, J. Yang and G. A. Ameer, *Expert Opin. Biol. Ther.*, 2004, **4**, 801–812.
2 L. Xue and H. P. Greisler, *J. Vasc. Surg.*, 2003, **37**, 472–480.
3 L. E. Millon, G. Guhados and W. Wan, *J. Biomed. Mater. Res., Part B*, 2008, **86b**, 444–452.
4 J. Yang, D. Motlagh, A. R. Webb and G. A. Ameer, *Tissue Eng.*, 2005, **11**, 1876–1886.
5 Y. Wang, G. A. Ameer, B. J. Sheppard and R. Langer, *Nat. Biotechnol.*, 2002, **20**, 602–606.
6 J. Yang, A. R. Webb and G. A. Ameer, *Adv. Mater.*, 2004, **16**, 511–516.
7 M. I. Almeida-Silveira, D. Lambertz, C. Perot and F. Goubel, *Eur. J. Appl. Physiol.*, 2000, **81**, 252–257.
8 Y. Wu, O. Cazorla, D. Labeit, S. Labeit and H. Granzier, *J. Mol. Cell. Cardiol.*, 2000, **32**, 2151–2162.
9 M. P. Lutolf, G. P. Raeber, A. H. Zisch, N. Tirelli and J. A. Hubbell, *Adv. Mater.*, 2003, **15**, 888–892.
10 J. A. Rowley, Z. Sun, D. Goldman and D. J. Mooney, *Adv. Mater.*, 2002, **14**, 886–889.
11 R. Langer and J. P. Vacanti, *Science*, 1993, **260**, 920–926.
12 M. Vert, *Med. J. Malays.*, 2004, **59**(Suppl B), 73–74.
13 A. G. Mikos, Y. Bao, L. G. Cima, D. E. Ingber, J. P. Vacanti and R. Langer, *J. Biomed. Mater. Res.*, 1993, **27**, 183–189.
14 R. L. Carrier, M. Papadaki, M. Rupnick, F. J. Schoen, N. Bursac, R. Langer, L. E. Freed and G. Vunjak-Novakovic, *Biotechnol. Bioeng.*, 1999, **64**, 580–589.
15 B. D. Ratner and S. J. Bryant, *Annu. Rev. Biomed. Eng.*, 2004, **6**, 41–75.
16 H. Zhao and G. A. Ameer, *J. Appl. Polym. Sci.*, 2009, **114**, 1464–1470.
17 R. T. Tran, Y. Zhang, D. Gyawali and J. Yang, *Recent Pat. Biomed. Eng.*, 2010, **2**, 216–227.
18 S. Atzet, S. Curtin, P. Trinh, S. Bryant and B. Ratner, *Biomacromolecules*, 2008, **9**, 3370–3377.
19 K. T. Nguyen and J. L. West, *Biomaterials*, 2002, **23**, 4307–4314.
20 K. Y. Lee and D. J. Mooney, *Chem. Rev.*, 2001, **101**, 1869–1879.
21 J. Kim, K. W. Lee, T. E. Hefferan, B. L. Currier, M. J. Yaszemski and L. Lu, *Biomacromolecules*, 2008, **9**, 149–157.
22 Y. Qiu and K. Park, *Adv. Drug Delivery Rev.*, 2001, **53**, 321–339.
23 C. L. Nijst, J. P. Bruggeman, J. M. Karp, L. Ferreira, A. Zumbuehl, C. J. Bettinger and R. Langer, *Biomacromolecules*, 2007, **8**, 3067–3073.
24 L. J. Suggs, E. Y. Kao, L. L. Palombo, R. S. Krishnan, M. S. Widmer and A. G. Mikos, *J. Biomater.Sci., Polym. Ed.*, 1998, **9**, 653–666.
25 S. R. Van Tomme, G. Storm and W. E. Hennink, *Int. J. Pharm.*, 2008, **355**, 1–18.
26 J. P. Fisher, M. D. Timmer, T. A. Holland, D. Dean, P. S. Engel and A. G. Mikos, *Biomacromolecules*, 2003, **4**, 1327–1334.
27 D. E. Noga, T. A. Petrie, A. Kumar, M. Weck, A. J. Garcia and D. M. Collard, *Biomacromolecules*, 2008, **9**, 2056–2062.
28 J. Yang, A. R. Webb, S. J. Pickerill, G. Hageman and G. A. Ameer, *Biomaterials*, 2006, **27**, 1889–1898.
29 M. Lang and C.-C. Chu, *J. Appl. Polym. Sci.*, 2002, **86**, 2296–2306.
30 S. H. Kim, C. Y. Won and C. C. Chu, *J. Biomed. Mater. Res.*, 1999, **46**, 160–170.
31 B. Guo, J. Yuan and Q. Gao, *Colloids Surf., B*, 2007, **58**, 151–156.
32 T. Pompe, S. Zschoche, N. Herold, K. Salchert, M. F. Gouzy, C. Sperling and C. Werner, *Biomacromolecules*, 2003, **4**, 1072–1079.
33 S. Harrisson and K. L. Wooley, *Chem. Commun.*, 2005, 3259–3261.

34 J. Dey, H. Xu, J. Shen, P. Thevenot, S. R. Gondi, K. T. Nguyen, B. S. Sumerlin, L. Tang and J. Yang, *Biomaterials*, 2008, **29**, 4637–4649.
35 J. P. Fisher, T. A. Holland, D. Dean and A. G. Mikos, *Biomacromolecules*, 2003, **4**, 1335–1342.
36 S. Tanodekaew, S. Channasanon and P. Uppanan, *J. Appl. Polym. Sci.*, 2006, **100**, 1914–1918.
37 W. Zhu and J. Ding, *J. Appl. Polym. Sci.*, 2006, **99**, 2375–2383.
38 D. A. Solovjov, E. Pluskota and E. F. Plow, *J. Biol. Chem.*, 2004, **280**, 1336–1345.
39 P.-J. Shi, Y.-G. Li and C.-Y. Pan, *Eur. Polym. J.*, 2004, **40**, 1283–1290.
40 D. Gyawali, R. T. Tran, K. Guleserian, L. Tang and J. Yang, *J. Biomater. Sci., Polym. Ed.*, 2010, **1**, DOI: 10.1163/092050609X12567178204169.
41 J. Guan, M. S. Sacks, E. J. Beckman and W. R. Wagner, *Biomaterials*, 2004, **25**, 85–96.
42 J. Yang, Y. Wan, J. Bei and S. Wang, *J. Biomed. Mater. Res.*, 2003, **67a**, 1139–1147.
43 Z. Chen, S. Cheng and K. Xu, *Biomaterials*, 2009, **30**, 2219–2230.
44 C. J. Bettinger, B. Orrick, A. Misra, R. Langer and J. T. Borenstein, *Biomaterials*, 2006, **27**, 2558–2565.
45 I. Levental, P. C. Georges and P. A. Janmey, *Soft Matter*, 2007, **3**, 299–306.
46 A. Jacinto, A. Martinez-Arias and P. Martin, *Nat. Cell Biol.*, 2001, **3**, E117–E123.
47 A. K. Burkoth and K. S. Anseth, *Biomaterials*, 2000, **21**, 2395–2404.
48 T. R. Kyriakides, M. J. Foster, G. E. Keeney, A. Tsai, C. M. Giachelli, I. Clark-Lewis, B. J. Rollins and P. Bornstein, *Am. J. Pathol.*, 2004, **165**, 2157–2166.
49 L. Nair and C. Laurencin, *Prog. Polym. Sci.*, 2007, **32**, 762–798.
50 C. J. Bettinger, J. P. Bruggeman, J. T. Borenstein and R. S. Langer, *Biomaterials*, 2008, **29**, 2315–2325.
51 J. M. Anderson, A. Rodriguez and D. T. Chang, *Semin. Immunol.*, 2008, **20**, 86–100.
52 S. F. Badylak, J. E. Valentin, A. K. Ravindra, G. P. McCabe and A. M. Stewart-Akers, *Tissue Eng. A*, 2008, **14**, 1835–1842.
53 R. Bashir, *Adv. Drug Delivery Rev.*, 2004, **56**, 1565–1586.
54 A. Khademhosseini and R. Langer, *Biomaterials*, 2007, **28**, 5087–5092.